AIAA AVIATION Forum
June 25-29, 2018, Atlanta, Georgia
2018 Fluid Dynamics Conference

10.2514/6.2018-3221

Transient growth in oblique shock wave/laminar boundary layer interactions at Mach 5.92

Nathaniel Hildebrand*, Joseph W. Nichols†, and Graham V. Candler‡
University of Minnesota, Minneapolis, MN, 55455, USA

Mihailo R. Jovanović§
University of Southern California, Los Angeles, CA, 90089, USA

We investigate the nonmodal physical mechanisms responsible for transient growth in a hypersonic laminar boundary layer and in the interaction of this boundary layer with an incident oblique shock wave. The optimal disturbances and growth curves are computed using an adjoint looping approach. We validate this iterative approach by applying it to several parallel boundary layers that have been studied before in great detail. For these parallel flows, the lift-up effect is generally the dominant transient growth mechanism. However, for a Mach 5.92 spatially developing boundary layer, the inviscid Orr mechanism and convective instabilities are responsible for the large transient response. Furthermore, the optimal initial condition corresponding to the oblique shock wave/boundary layer interaction could be related to both the inviscid Orr mechanism and the lift-up effect. Tilted streamwise streaks that oppose the mean shear are present in the upstream boundary layer, and centrifugal instability near the apex of the separation bubble creates small vortices that grow into elongated streamwise structures with time. Due to the strong spatial non-normality of the oblique shock wave/boundary layer interaction, one cannot obtain an accurate lower bound of the transient growth using the direct or adjoint information separately. Therefore, the nonmodal technique, which takes advantage of both the direct and adjoint operators, is an elegant solution to this problem.

Nomenclature

(u, v, w)	streamwise, wall-normal, and spanwise velocity components	$\hat{\boldsymbol{q}}$	vector of amplitude variables
		κ	coefficient of heat conductivity
(x, y, z)	Cartesian coordinates	λ	second viscosity coefficient
α	streamwise wavenumber	$\mathcal{T}$	fixed time interval
$\bar{\boldsymbol{q}}$	vector of base flow variables	μ	dynamic viscosity
β	spanwise wavenumber	ν	kinematic viscosity
$\boldsymbol{\tau}$	viscous shear stress tensor	ω	temporal frequency
$\boldsymbol{I}$	identitiy matrix	ϕ	viscous dissipation
$\boldsymbol{q}$	vector of system variables	ρ	density
$\boldsymbol{q}'$	vector of perturbation variables	θ	incident shock angle
$\boldsymbol{u}$	velocity vector	a	speed of sound
δ	displacement thickness	E	disturbance energy
ℓ	alternate length scale	G	optimal transient energy growth
ϵ	filter strength	i	imaginary unit
γ	ratio of specific heats	L	domain length

*Graduate Research Assistant, UMN Aerospace Engineering and Mechanics, AIAA Student Member.
†Assistant Professor, UMN Aerospace Engineering and Mechanics, AIAA Member.
‡Russell J. Penrose and McKnight Presidential Professor, UMN Aerospace Engineering and Mechanics, AIAA Fellow.
§Professor, USC Electrical Engineering, APS Fellow.

M	Mach number
n	number of points
p	pressure
Pr	Prandtl number
Re	Reynolds number
s	entropy
T	temperature
t	time
W	weighting matrix

Subscripts

0	stagnation
∞	freestream value
E	with respect to energy norm
s	Sutherland value
in	inflow value

Superscripts

$*$	complex conjugate
$+$	viscous units
H	complex conjugate transpose
T	transpose

Abbreviatons

ACE	actively controlled expansion
DPLR	data-parallel line relaxation
GSA	global stability analysis
KEC	kinetic energy consistent
LNS	linearized Navier-Stokes
LU	lower upper
PSE	parabolized stability equations
SWBLI	shock wave/boundary layer interaction

I. Introduction

In order to improve the performance of a hypersonic vehicle, the stability of high-speed boundary layers and shock wave/boundary layer interactions (SWBLIs) has to be understood. More specifically, a deeper understanding of these flows and the development of better prediction tools can drastically reduce heat loads and skin friction drag on a vehicle's surface. Previous work has focused mainly on the exponential growth of perturbations corresponding to unstable eigenmodes for boundary layers[1−3] and SWBLIs[4−7] in different flow configurations. It has recently been demonstrated that nonmodal physical mechanisms in the flow can lead to a large transient growth of perturbations despite their eventual asymptotic decay.[8] Furthermore, this amplification could be strong enough to trigger nonlinear interactions that ultimately breakdown into turbulent flow (bypassing modal instabilities).[9,10]

The application of nonmodal growth analyses first appeared in the low-speed or incompressible regime.[11] Butler and Farrell[12] found by applying an optimal perturbation technique about plane channel flow that small disturbances, specifically elongated streamwise structures that oppose the specified mean shear flow, grow rapidly and robustly. These disturbances are often associated with the inviscid Orr mechanism.[13] The linear growth of initially small disturbances can eventually become nonlinear and lead to what is called bypass transition.[9] This can be seen with the presence of streamwise streaks on a Blasius boundary layer.[14,15] A more recent paper by Tempelmann et al.[16] showed that the physical mechanism driving nonmodal growth in three-dimensional boundary layers consists of the Landahl lift-up effect[17,18] and the Orr mechanism. Using the temporal framework, Hanifi et al.[19] applied transient growth analysis to compressible boundary layers for the first time. They showed that the optimal disturbances in compressible boundary layers are similar to those in the incompressible regime. Several other studies have applied transient growth analysis in the spatial framework,[20] while focusing on the inclusion of nonparallel flow effects.[21−23]

Optimal spatial and transient growth analyses have recently been applied to hypersonic flows. Bitter and Shepherd[8] investigated the importance of modal and nonmodal growth mechanisms in flat-plate hypersonic boundary layers. They also studied the effects of Mach number and wall cooling on these processes. By using both the temporal and spatial framework, they showed that the optimal disturbances consist of streamwise vortices, which develop into streaks of high velocity and temperature. Additional sub-optimal disturbances were found that had nonzero frequency and grew more rapidly than the optimal ones. Paredes et al.[24] utilized the parabolized stability equations (PSE) to study optimal transient growth in compressible zero-pressure-gradient boundary layer flows at Mach numbers ranging from 3 to 10. They found that as the Mach number increases, the differences between the optimal gain computed about a Navier-Stokes mean flow and a self-similar boundary layer approximation becomes significant. Paredes et al.[25] performed an optimal transient growth analysis about a laminar flow based on the solution of the Navier-Stokes equations over a 7° half-angle variable-bluntness cone at zero angle of attack. Their main conclusion is that disturbances initiated near the juncture between the nosetip and the frustum exhibit a greater transient amplification for larger values of nosetip bluntness. They also suggest that wall roughness might be able to induce optimal initial perturbations.

Literature related to the application of spatial or transient growth analysis to SWBLIs is relatively sparse. A recent study by Guiho et al.[26] investigated the interaction of an oblique shock wave with a laminar Mach 2.15 boundary layer by means of numerical simulation and global stability analysis (GSA). They showed that the unsteadiness of a SWBLI is mainly associated with instabilities arising from the shear layer. In this study, they also looked at the receptivity of their SWBLI to a white noise excitation. They concluded by suggesting a SWBLI behaves similar to a selective noise amplifier in that its dynamics are driven mainly by receptivity mechanisms and a nonmodal transient response. Dwivedi et al.[27] measured the spatial growth of streamwise streaks in a Mach 5.92 SWBLI using an adjoint looping PSE-based algorithm. In this conference paper, they highlight the importance of centrifugal instability to the development of streamwise streaks and large spatial growth in a SWBLI. Sartor et al.[28] experimentally and theoretically examined unsteadiness in transonic shock wave/turbulent boundary layer interactions. They briefly showed that these types of interactions can potentially lead to large transient growth.

Our work focuses on applying an optimal transient growth analysis to a Mach 5.92 nonparallel laminar boundary layer as well as to the interaction of that boundary layer with an oblique shock wave. This will shed light on the different types of modal and nonmodal disturbances an experimentalist can measure in an oblique SWBLI laboratory setup. It also provides some insight on the topic of whether nonmodal growth mechanisms can excite nonlinear interactions that lead to transition (bypassing modal instabilities). We compute the optimal disturbances and growth curves using an adjoint looping approach in time.[29] This iterative approach is validated against the results of Hanifi et al.,[19] which looked at parallel boundary layer profiles. For every flow configuration, we illustrate and describe the physical mechanism that causes the transient growth. We also determine if it is related to the Landahl lift-up effect[17,18] or the inviscid Orr mechanism[13] both of which present in many boundary layer flows. Finally, we want to compare the relative magnitude and dominant spanwise wavenumber of the optimal transient energy growth of a SWBLI to that of a nonparallel boundary layer.

II. Problem formulation

A. Flow configuration

In this study, we simulate a hypersonic laminar boundary layer and the interaction of that boundary layer with an oblique shock wave. Figure 1 shows a schematic of a canonical SWBLI. High-speed freestream flow enters at the left boundary and flows over a flat plate situated along the bottom boundary. For this configuration, the leading edge of the flat plate is upstream of the left boundary and produces a bow shock that persists throughout the domain. At the inflow, the boundary layer has displacement thickness δ_{in} and slowly grows as it develops downstream (refer to Shrestha et al.[30] for details). Also, an oblique shock wave enters the domain through the left boundary well above both the bow shock and the boundary layer. Such an oblique shock wave might result from placing a turning wedge in the freestream a distance upstream. The incident oblique shock wave propagates at an angle θ until it impinges on the boundary layer. The adverse pressure gradient of the impinging shock causes the boundary layer to separate from the wall and form a recirculation bubble. For simulations of just the hypersonic laminar boundary layer, the incident shock and recirculation bubble do not appear, but the bow shock is still present.

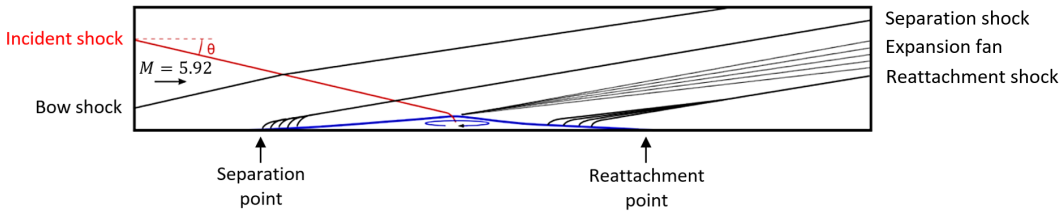

Figure 1: Schematic of an oblique shock wave (red) impinging on a Mach 5.92 boundary layer. The adverse pressure gradient associated with the incident shock causes the boundary layer to separate from the wall, forming a recirculation bubble (blue).

We consider freestream flow conditions matching experiments performed in the ACE Hypersonic Wind Tunnel at Texas A&M University.[31] Between the bow shock and the incident shock, the freestream Mach

number, temperature, and pressure are $M_\infty = 5.92$, $T_\infty = 53.06$ K, and $p_\infty = 308.2$ Pa, respectively. A Reynolds number of $Re = \rho_\infty u_\infty \delta_{\text{in}}/\mu_\infty = 9660$ based on the undisturbed boundary layer displacement thickness $\delta_{\text{in}} = 2.1$ mm at the inflow is used in the present study. This corresponds to a unit Reynolds number of 4.6×10^6 m^{-1}. Here ρ_∞, u_∞, and μ_∞ denote the freestream density, velocity, and dynamic viscosity, respectively. A Cartesian coordinate system is utilized hereafter with x, y, and z denoting the streamwise, wall-normal, and spanwise directions, respectively.

B. Governing equations

The compressible Navier-Stokes equations are used to mathematically model the dynamics of a nonparallel boundary layer and an oblique SWBLI at hypersonic speeds. These equations govern the evolution of the system state $\boldsymbol{q} = [p;\, \boldsymbol{u}^{\mathrm{T}};\, s]^{\mathrm{T}}$, where p, $\boldsymbol{u}$, and s are the non-dimensional fluid pressure, velocity vector, and entropy, respectively.[32,33] After nondimensionalization with respect to the displacement thickness δ_{in}, freestream velocity u_∞, density ρ_∞, and temperature T_∞, these equations are written as

$$\frac{\partial p}{\partial t} + \boldsymbol{u}\cdot\boldsymbol{\nabla} p + \rho a^2 \boldsymbol{\nabla}\cdot\boldsymbol{u} = \frac{1}{Re}\left[\frac{1}{M_\infty^2 Pr}\boldsymbol{\nabla}\cdot(\mu\boldsymbol{\nabla}T) + (\gamma-1)\phi\right], \tag{1a}$$

$$\frac{\partial \boldsymbol{u}}{\partial t} + \frac{1}{\rho}\boldsymbol{\nabla} p + \boldsymbol{u}\cdot\boldsymbol{\nabla}\boldsymbol{u} = \frac{1}{Re}\frac{1}{\rho}\boldsymbol{\nabla}\cdot\boldsymbol{\tau}, \tag{1b}$$

$$\frac{\partial s}{\partial t} + \boldsymbol{u}\cdot\boldsymbol{\nabla} s = \frac{1}{Re}\frac{1}{\rho T}\left[\frac{1}{(\gamma-1)M_\infty^2 Pr}\boldsymbol{\nabla}\cdot(\mu\boldsymbol{\nabla}T) + \phi\right]. \tag{1c}$$

The time scales are normalized by $\delta_{\text{in}}/u_\infty$ and pressure with $\rho_\infty u_\infty^2$. For an ideal fluid, the density ρ and temperature T are related to pressure p through the equation of state $\gamma M_\infty^2 p = \rho T$. The freestream Mach number is defined as $M_\infty = U_\infty/a_\infty$, where $a_\infty = \sqrt{\gamma p_\infty/\rho_\infty}$ is the speed of sound in the freestream. Furthermore, $\gamma = 1.4$ is the assumed constant ratio of specific heats.

We define entropy as $s = \ln(T)/[(\gamma-1)M_\infty^2] - \ln(p)/(\gamma M_\infty^2)$ so that $s = 0$ when $p = 1$ and $T = 1$. The viscous stress tensor $\boldsymbol{\tau}$ is written in terms of the identity matrix $\boldsymbol{I}$, velocity vector $\boldsymbol{u}$, and dynamic viscosity μ to yield the following expression

$$\boldsymbol{\tau} = \mu[\boldsymbol{\nabla}\boldsymbol{u} + (\boldsymbol{\nabla}\boldsymbol{u})^{\mathrm{T}} - \frac{2}{3}(\boldsymbol{\nabla}\cdot\boldsymbol{u})\boldsymbol{I}]. \tag{2}$$

The viscous dissipation is defined as $\phi = \boldsymbol{\tau} : \boldsymbol{\nabla}\boldsymbol{u}$. Note that the operator $:$ represents a scalar or double dot product between two tensors. Furthermore, the second viscosity coefficient is set to $\lambda = -2\mu/3$. In order to compute the dynamic viscosity μ, Sutherland's law is used with $T_s = 110.3$ K as follows

$$\mu(T) = T^{3/2}\frac{1 + T_s/T_\infty}{T + T_s/T_\infty}. \tag{3}$$

The Prandtl number is set to $Pr = \mu(T)/\kappa(T) = 0.72$, where $\kappa(T)$ is the coefficient of heat conductivity.

C. Linearized model

To investigate the behavior of small fluctuations about various base flows, system (1) is linearized by decomposing the state variables $\boldsymbol{q} = \bar{\boldsymbol{q}} + \boldsymbol{q}'$ into steady and fluctuating parts. By keeping only the first-order terms in $\boldsymbol{q}'$, the linearized Navier-Stokes (LNS) equations are obtained

$$\begin{aligned}\frac{\partial p'}{\partial t} + \bar{\boldsymbol{u}}\cdot\boldsymbol{\nabla} p' + \boldsymbol{u}'\cdot\boldsymbol{\nabla}\bar{p} + \bar{\rho}\bar{a}^2\boldsymbol{\nabla}\cdot\boldsymbol{u}' + \gamma(\boldsymbol{\nabla}\cdot\bar{\boldsymbol{u}})p' = \frac{1}{Re}\Bigg\{&\frac{1}{M_\infty^2 Pr}\boldsymbol{\nabla}\cdot(\bar{\mu}\boldsymbol{\nabla}T' + \mu'\boldsymbol{\nabla}\bar{T}) \\ &+ (\gamma-1)\left[\bar{\boldsymbol{\tau}} : \boldsymbol{\nabla}\boldsymbol{u}' + \boldsymbol{\tau}' : \boldsymbol{\nabla}\bar{\boldsymbol{u}}\right]\Bigg\},\end{aligned} \tag{4a}$$

$$\frac{\partial \boldsymbol{u}'}{\partial t} + \frac{1}{\bar{\rho}}\boldsymbol{\nabla} p' - \frac{\rho'}{\bar{\rho}^2}\boldsymbol{\nabla}\bar{p} + \bar{\boldsymbol{u}}\cdot\boldsymbol{\nabla}\boldsymbol{u}' + \boldsymbol{u}'\cdot\boldsymbol{\nabla}\bar{\boldsymbol{u}} = \frac{1}{Re}\left\{\frac{1}{\bar{\rho}}\boldsymbol{\nabla}\cdot\boldsymbol{\tau}' - \frac{\rho'}{\bar{\rho}^2}\boldsymbol{\nabla}\cdot\bar{\boldsymbol{\tau}}\right\}, \tag{4b}$$

$$\frac{\partial s'}{\partial t} + \bar{\boldsymbol{u}} \cdot \boldsymbol{\nabla} s' + \boldsymbol{u}' \cdot \boldsymbol{\nabla} \bar{s} = \frac{1}{Re} \frac{1}{\bar{\rho}\bar{T}} \Bigg\{ \frac{1}{(\gamma-1) M_\infty^2 Pr} \left[\boldsymbol{\nabla} \cdot (\bar{\mu} \boldsymbol{\nabla} T' + \mu' \boldsymbol{\nabla} \bar{T}) - \frac{p'}{\bar{p}} \boldsymbol{\nabla} \cdot (\bar{\mu} \boldsymbol{\nabla} \bar{T}) \right] + \bar{\boldsymbol{\tau}} : \boldsymbol{\nabla} \boldsymbol{u}' + \boldsymbol{\tau}' : \boldsymbol{\nabla} \bar{\boldsymbol{u}} - \frac{p'}{\bar{p}} \bar{\boldsymbol{\tau}} : \boldsymbol{\nabla} \bar{\boldsymbol{u}} \Bigg\}. \tag{4c}$$

The overbars and primes denote the base flow and fluctuating parts, respectively. Moreover, the equation of state is linearized to obtain $\rho'/\bar{\rho} = p'/\bar{p} - T'/\bar{T}$. The expression $T' = (\gamma-1) M_\infty^2 (\bar{T} s' + p'/\bar{\rho})$ is derived by linearizing the definition of entropy and substituting in the equation of state. The perturbed viscous stress tensor is given by

$$\boldsymbol{\tau}' = \bar{\mu} [\boldsymbol{\nabla} \boldsymbol{u}' + (\boldsymbol{\nabla} \boldsymbol{u}')^{\mathrm{T}} - \frac{2}{3} (\boldsymbol{\nabla} \cdot \boldsymbol{u}') \boldsymbol{I}] + \mu' [\boldsymbol{\nabla} \bar{\boldsymbol{u}} + (\boldsymbol{\nabla} \bar{\boldsymbol{u}})^{\mathrm{T}} - \frac{2}{3} (\boldsymbol{\nabla} \cdot \bar{\boldsymbol{u}}) \boldsymbol{I}], \tag{5}$$

and the perturbed dynamic viscosity is given by $\mu' = (\partial \bar{\mu} / \partial \bar{T}) T'$. We verified the accuracy of this characteristic formulation in Hildebrand et al.[7] by comparing our results from GSA to Malik's stability analysis[34] of parallel high-speed boundary layers.

Global modes of the linear system (4) take the form

$$\boldsymbol{q}'(x, y, z, t) = \hat{\boldsymbol{q}}(x, y) e^{i(\beta z - \omega t)}, \tag{6}$$

where β is the nondimensional spanwise wavenumber and ω is the temporal frequency. Substitution of (6) into (4) yields the eigenvalue problem

$$A \hat{\boldsymbol{q}} = -i\omega \hat{\boldsymbol{q}}. \tag{7}$$

The operator A, known as the Jacobian operator, includes all terms in system (4) that do not involve a time derivative. The Jacobian operator gives the linear variation of the residual (i.e., terms without a time derivative) of the original nonlinear system (1) with respect to the state variables, taken about a base flow.

D. Adjoint looping method

Previous studies have predominately used a modal singular value decomposition to compute the transient growth in a variety of different flow configurations (including boundary layers,[8,19] supersonic jets,[33] and open channel flows[35]). This involves taking a non-normal superposition of the eigenvalues and eigenvectors of a system. One major problem with using a singular value decomposition is that for certain flows it takes thousands of eigenmodes to reach a converged solution.[36] Therefore, this way of computing the transient growth can be extremely memory intensive.

In this study, we use an iterative approach that utilizes the Jacobian operator A and its adjoint A^{H} to compute the transient growth.[29] For a discussion on adjoint operators and their properties see the review by Luchini and Bottaro.[37] We define the disturbance energy as

$$E = \iint \left[\frac{\bar{\rho} u_i' u_i'^*}{2} + \frac{M_\infty^2 |p'|^2}{2} + \frac{(\gamma-1) M_\infty^2 |s'|^2}{2} \right] \mathrm{d}x \mathrm{d}y, \tag{8}$$

where * signifies the complex conjugate. This useful measure for compressible flows is positive definite and monotone nonincreasing.[38] It is independently derived in Hanifi et al.[19] by eliminating conservative compression work transfer terms. The expression (8) induces the following inner product $(\boldsymbol{q}_1, \boldsymbol{q}_2)_E = \boldsymbol{q}_2^{\mathrm{H}} W \boldsymbol{q}_1$ for two system states $\boldsymbol{q}_1$ and $\boldsymbol{q}_2$, where $W = 1/2 \ \mathrm{diag}[M^2, \bar{\rho}, \bar{\rho}, \bar{\rho}, \gamma(\gamma-1)M^2] \Delta x \Delta y$. We define $G(t)$ to be the largest amplification at time t such that

$$G(t) = \max \frac{||\boldsymbol{q}(t)||_E^2}{||\boldsymbol{q}(0)||_E^2}, \tag{9}$$

where $\boldsymbol{q}(0)$ and $\boldsymbol{q}(t)$ represent the initial and final states, respectively. The adjoint looping method uses a reformulation of the optimal energy growth $G(t)$ in terms of a variational principle.[39] Standard optimization techniques can then be employed to arrive at the optimal initial and final states in an iterative manner. The

optimization process should respect the constraints given by the LNS equations (4). These constraints are enforced via Lagrange multipliers.[40]

During one cycle of this iterative process, the LNS equations (4) are integrated forward in time using a given initial condition. After a fixed time interval $t = \mathcal{T}$, the output of this integration $\boldsymbol{q}(\mathcal{T})$ is converted into a terminal condition $\widetilde{\boldsymbol{q}}(\mathcal{T})$ for the adjoint equations. Next, we solve the adjoint equations backward in time to produce a state $\widetilde{\boldsymbol{q}}(0)$ from which a new initial condition $\boldsymbol{q}(0)$ for the direct problem is obtained. This procedure is repeated until convergence. Figure 2 shows a detailed sketch of the adjoint looping method including the updates between each time integration scheme. The final result is the initial condition that maximizes the amplification of energy over a time interval $0 \leq t \leq \mathcal{T}$, from which the maximum transient growth $G(t)$ is readily determined.[39] Similar adjoint looping techniques have been successfully implemented in various complex boundary layer flows.[41,42]

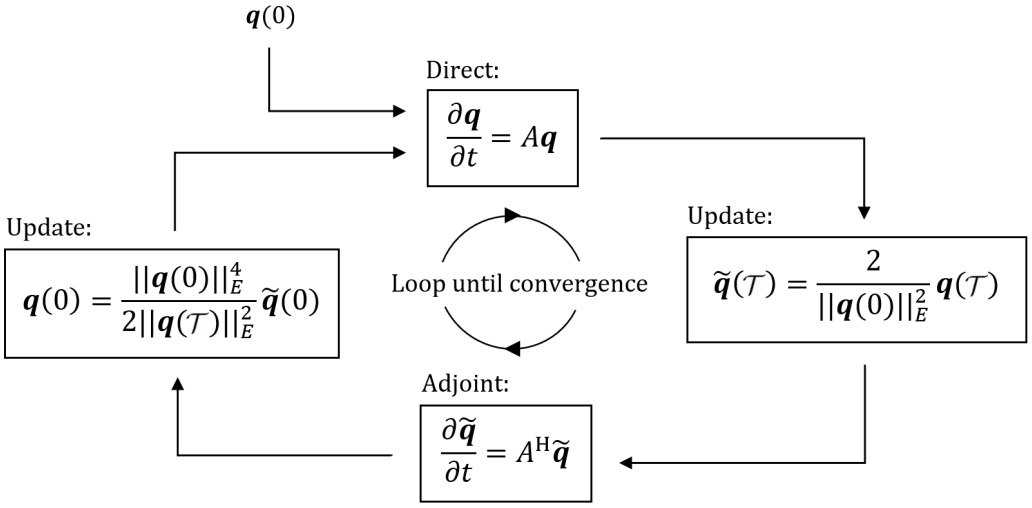

Figure 2: A detailed sketch of the adjoint looping method used in this study.

E. Numerics

We solve the compressible Navier-Stokes equations in conservative form for the base flow calculations of the nonparallel boundary layers and oblique SWBLIs.[30] A stable low-dissipation scheme based upon the kinetic energy consistent (KEC) method developed by Subbareddy and Candler[43] is implemented for the inviscid flux computation. In this numerical method, the flux is split into a symmetric (or non-dissipative) portion and an upwind (or dissipative) portion. The inviscid flux is premultiplied by a shock-detecting switch, which ensures that dissipation occurs only around shocks.[44] A fourth-order centered KEC scheme is employed for the present study. Viscous fluxes are modeled with second-order central differences. Time integration is performed using an implicit second-order Euler method with point relaxation to maintain numerical stability.[45] The implicit system is also solved using the full matrix data-parallel line relaxation (DPLR) method, which has good parallel efficiency.[46]

For the transient growth calculations, the LNS equations (4) are discretized by fourth-order centered finite differences applied on a stretched mesh. This results in a large sparse matrix.[53] Time integration is performed using an implicit first-order Euler method. The inversion step is computed by finding the LU decomposition of the shifted sparse matrix with the massively parallel SuperLU package.[48] We use a Newton-Raphson method to converge the residual of each base flow in accordance with system (1) to machine zero. This mitigates any error introduced by going from a conservative formulation[45] to a nonconservative or characteristic formulation[32] when computing the transient growth. A numerical filter is used to add minor amounts of scale-selective artificial dissipation to damp spurious modes associated with the smallest wavelengths allowed by the mesh. We introduce the numerical filter by adding terms of the form $\epsilon(\partial^4 \boldsymbol{q}/\partial x^4)$ and $\epsilon(\partial^4 \boldsymbol{q}/\partial y^4)$. Here, the filter strength ϵ is set to 0.0125, its smallest value such that the Newton-Raphson method still converges. Sponge layers are employed at the top, left, and right boundaries of the nonparallel boundary layer and oblique SWBLI flows to absorb outgoing information with minimal reflection.[49]

III. RESULTS

A. Parallel boundary layers

To verify our adjoint looping method, we run a few test cases that are presented in Hanifi et al.[19] The base flow is locally parallel and consists of a boundary layer profile that satisfies the Mangler-Levy-Lees transformation. We model the bottom boundary as an adiabatic wall. Furthermore, we employ periodicity at the left and right boundaries of the domain. A sponge layer is placed along the top boundary, which we treat as a freestream outlet. Further, we use a stretched grid with $(n_x, n_y) = (101, 301)$ and $y^+ = 0.6$ for every case. We define a new length scale $\ell = \sqrt{\nu_\infty x/u_\infty}$, where ν_∞ is the kinematic viscosity in the freestream. For these parallel boundary layer calculations only, we use a Prandtl number of $Pr = 0.7$ and a stagnation temperature of $T_0 = 333$ K.

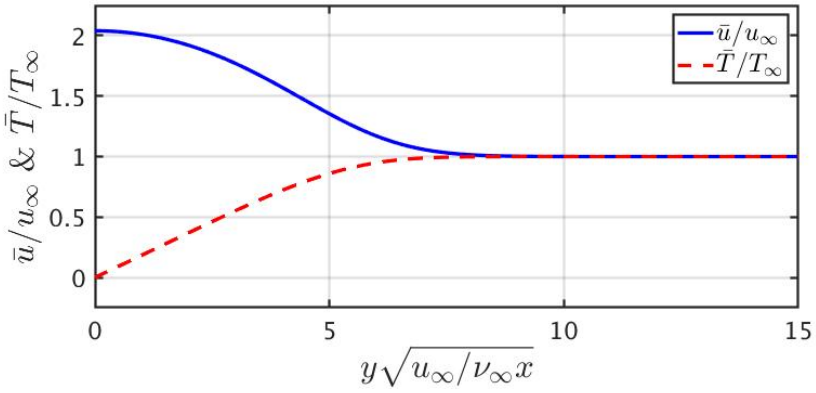

Figure 3: Base flow profiles of a locally parallel Mach 2.5 boundary layer with $Re_\ell = 3000$.

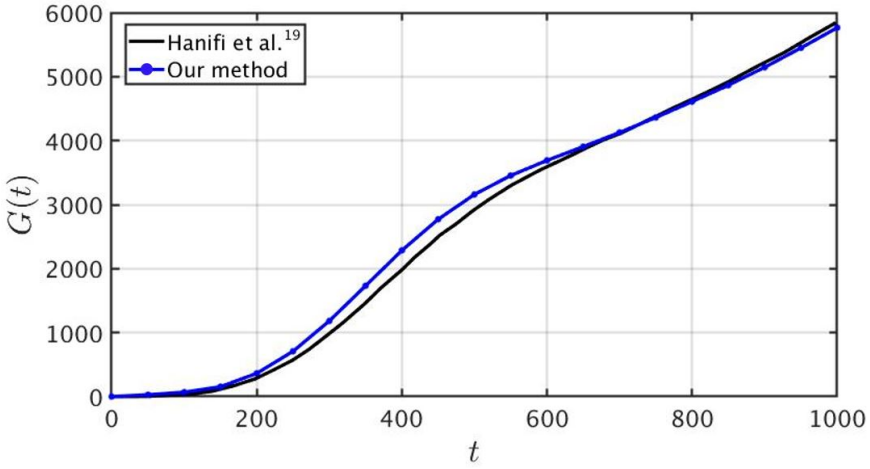

Figure 4: Envelope of the optimal transient energy growth for a locally parallel Mach 2.5 boundary layer with $Re_\ell = 3000$, $\alpha = 0.06$, and $\beta = 0.1$.

First, we consider the case where $M_\infty = 2.5$, $Re = 3000$, $\alpha = 0.06$, and $\beta = 0.1$. Here, the Reynolds number is with respect to the length scale ℓ, and we denote α as the nondimensional streamwise wavenumber. Figure 3 shows the boundary layer profiles for this case. We generate a two-dimensional parallel flow by copying these boundary layer profiles in the streamwise direction. To calculate the streamwise domain length, we use the relation $L_x = 2\pi/\alpha$. We compute the optimal transient energy growth of this parallel boundary layer flow with the adjoint looping approach described in Section IID. The given initial condition to start the iterative process in Figure 2 is a randomly generated flow field with unit energy norm. To make

sure the given randomly generated initial condition has wavenumber $\alpha = 0.06$ only, we perform fast Fourier transforms (FFTs) in the streamwise direction and keep only the coefficients corresponding to the specified nondimensional streamwise wavenumber. After, we transform back to physical space.

Figure 4 compares the transient growth $G(t)$ that results from the adjoint looping approach to the singular value decomposition used in Hanifi et al.[19] Note that $G(t)$ is an envelope of all possible optimal responses, since the optimum initial condition $\boldsymbol{q}(0)$ depends on the finite time interval t considered. The iterative procedure in Figure 2 takes approximately 5-6 iterations to converge (see Appendix) to just a single value of $G(t)$. Therefore, to trace out the entire envelope, we have to repeat this procedure for many different time intervals t (represented by blue dots in Figure 4). We see fairly good agreement between the two transient growth envelopes in Figure 4 computed from different methods. The slight disagreement around $t = 450$ could be due to very small numerical error contaminating the solution such that we are not constrained to a single streamwise wavenumber. Hanifi et al.[19] solves for the transient growth $G(t)$ in one spatial dimension so there is no way of resolving more than one streamwise wavenumber. Regardless, both methods converge to the same envelope shape with the global instability[19] starting to take over at $t = 1000$.

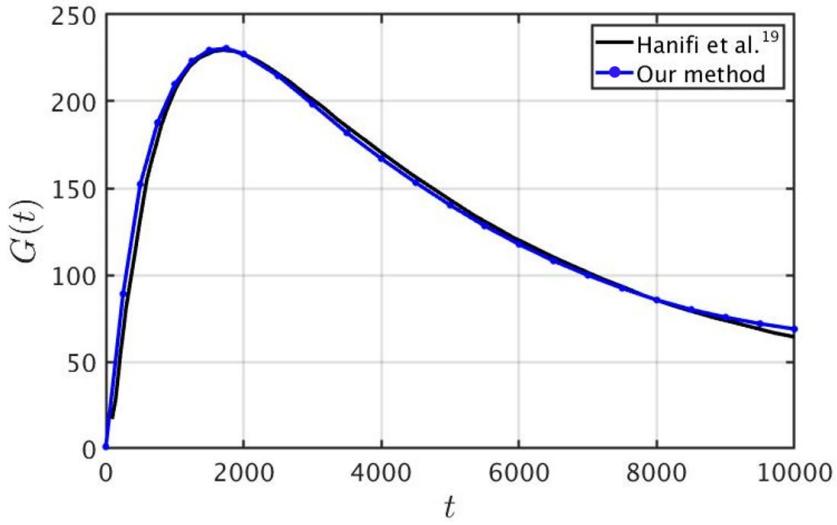

Figure 5: Envelope of the optimal transient energy growth for a locally parallel Mach 2.5 boundary layer with $Re_\ell = 300$, $\alpha = 0.0$, and $\beta = 0.1$.

We repeat the same transient growth analysis for the case where $M_\infty = 2.5$, $Re = 300$, $\alpha = 0.0$, and $\beta = 0.1$. Figure 5 shows the transient growth envelope for this case. Again we compare to the results in Hanifi et al.[19] There is excellent agreement between the adjoint looping method and the singular value decomposition in Figure 5. Notice there is a clear peak at $t = 1750$, after which the transient growth $G(t)$ decreases with increasing time t. We plot the optimal initial and final states corresponding to the peak at $t = 1750$ in Figure 6. The optimal initial condition consists mostly of wall-normal and spanwise velocities, while the streamwise velocity is negligible. This type of initial state has been seen for many incompressible[9,12] and compressible[20,21] flows. The disturbances in Figure 6 have been scaled to have a maximum of one, but the final state has actually grown by about two orders of magnitude relative to the initial state.[8] In the final state, the streamwise velocity is extremely large compared to the other velocity components. The physical interpretation of this amplification is the well-known Landahl lift-up effect.[17,18] This is where initial streamwise vortices that have relatively small u' and T' decay in time, while elongated streamwise structures grow rapidly.

Finally, we repeat the same transient growth analysis with $M_\infty = 2.5$, $Re = 300$, $\alpha = 0.0$, and $\beta = 0.25$. This case corresponds to the optimal streamwise and spanwise wavenumbers reported in Hanifi et al.[19] for $M_\infty = 2.5$ and $Re = 300$. We only show the initial and final states in Figure 7 to compare against the results of Hanifi et al.[19] There is great agreement between the two different approaches for the optimal initial and final states in Figure 7. Notice that the final state has grown three orders of magnitude relative to the initial state. We see along with the streamwise velocity, the temperature fluctuations are a vital component to the Landahl lift-up effect[17,18] for an adiabatic wall. Since we get good agreement comparing

the transient growth envelopes as well as the optimal initial and final states from our adjoint looping method to the results computed by a singular value decomposition in Hanifi et al.,[19] we conclude that our method accurately computes the transient response of high-speed parallel boundary layers.

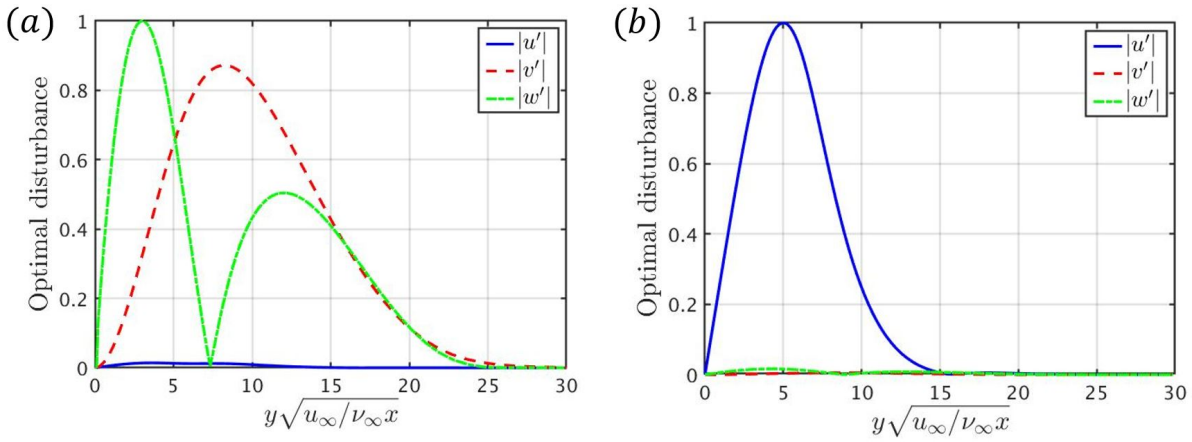

Figure 6: Optimal (a) initial and (b) final states corresponding to Figure 5, where $M_\infty = 2.5$, $Re_\ell = 300$, $\alpha = 0.0$, and $\beta = 0.1$.

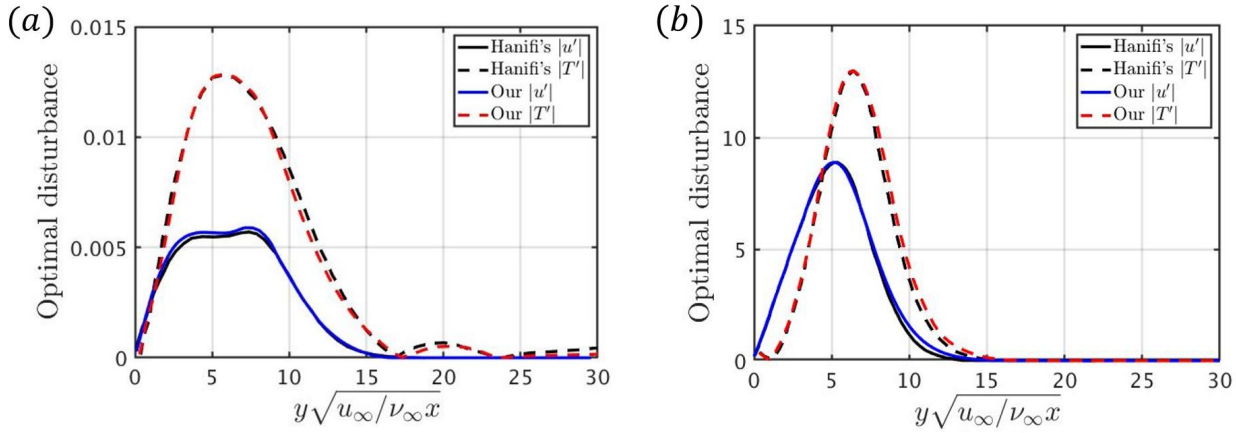

Figure 7: Optimal (a) initial and (b) final states for a locally parallel boundary layer with $M_\infty = 2.5$, $Re_\ell = 300$, $\alpha = 0.0$, and $\beta = 0.25$.

B. Spatially developing boundary layers

Since the transient growth of parallel boundary layers has been studied before, and we have successfully verified our adjoint looping method against these studies, we now focus our efforts on investigating the transient growth of nonparallel boundary layers. Bitter[50] recently looked at the propagation of localized instability wave packets in nonparallel boundary layers. This study included a conventional spatial stability analysis involving fixed-frequency disturbances, examining the development of Gaussian-shaped packets of second mode waves that are placed inside the boundary layer, and analyzing the response of planar acoustics wave packets in the freestream. All of the simulations in Bitter[50] show that finite-width wave packets experience less amplification than the prediction of spatial stability analysis.

In order to conduct an optimal transient growth analysis of nonparallel boundary layers, we first need to compute a steady two-dimensional base flow. The domain we consider extends $235\delta_{in}$ in the streamwise direction and $36\delta_{in}$ in the wall-normal direction. Our domain is discretized by a Cartesian mesh that is stretched in the wall-normal direction with $y^+ = 0.6$ and uniformly spaced in the streamwise direction. A

total of $n_x = 998$ and $n_y = 450$ grid points resolve the domain in the streamwise and wall-normal directions, respectively. The base flow simulations are run for approximately 60 flow-through times with the US3D hypersonic flow solver[51] until the residual is on the order of machine zero. Here a flow-through time is defined as the time it takes for a fluid particle to traverse the entire streamwise length of the domain, traveling with the freestream at Mach 5.92.

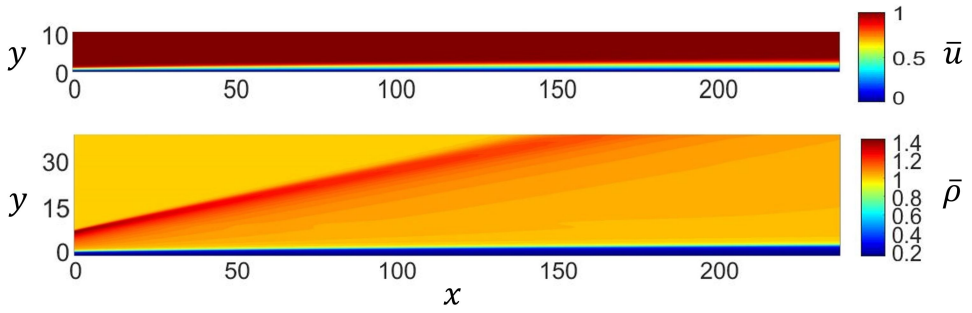

Figure 8: Base flow contours of streamwise velocity and density for a Mach 5.92 spatially developing boundary layer with $Re_{\delta_{in}} = 9660$.

Figure 8 shows base flow contours of the spatially developing boundary layer we consider in this section. At the left inlet, we apply boundary layer profiles computed from an earlier study.[30] This produces a bow shock and an entropy layer in close vicinity. The lower boundary is modeled as an adiabatic wall. We enforce a hypersonic freestream inlet along the top edge of the domain. Furthermore, we impose a characteristic-based supersonic outlet boundary condition along the right edge of the domain. Notice in Figure 8 that the boundary layer grows substantially in the streamwise direction.

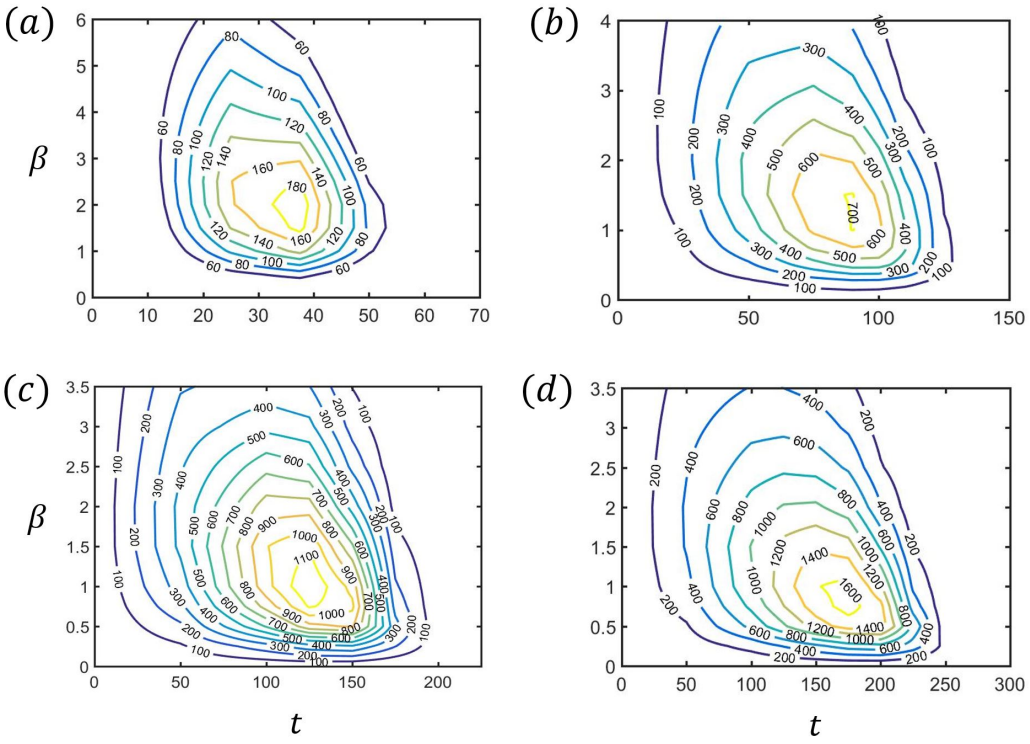

Figure 9: Contour plots of the transient growth $G(\beta, t)$ of a Mach 5.92 spatially developing boundary layer with $Re_{\delta_{in}} = 9660$ for streamwise extents equal to (a) $58.75\delta_{in}$, (b) $117.5\delta_{in}$, (c) $176.25\delta_{in}$, and (d) $235\delta_{in}$.

Now we compute the optimal transient energy growth of the spatially developing boundary layer in Figure 8 with our adjoint looping method. The given initial condition to start this iterative process is a randomly generated flow field with unit energy norm like before. For this case, we are no longer constrained to a single streamwise wavenumber. The iterative process in Figure 2 takes roughly 5-6 iterations to converge (see Appendix). Figure 9 shows the transient growth over a range of time intervals t, nondimensional spanwise wavenumbers β, and streamwise domain lengths L_x. We see that as the streamwise extent of the domain increases, the optimal transient growth becomes significantly larger. This indicates that a Mach 5.92 spatially developing boundary layer is convectively unstable. In other words, localized perturbations introduced upstream will grow as they convect downstream without causing the system to become globally (or absolutely) unstable.[52,53] Thus, if a high-speed boundary layer is allowed to develop more downstream, then the response to any upstream initial condition will be much larger. The spanwise wavenumber that corresponds to the maximum transient growth in Figure 9 decreases from $\beta = 1.95$ for $L_x = 58.75\delta_{in}$ to $\beta = 0.75$ for $L_x = 235\delta_{in}$. We also see that the transient growth is sustained for a much longer time if the streamwise domain length is larger.

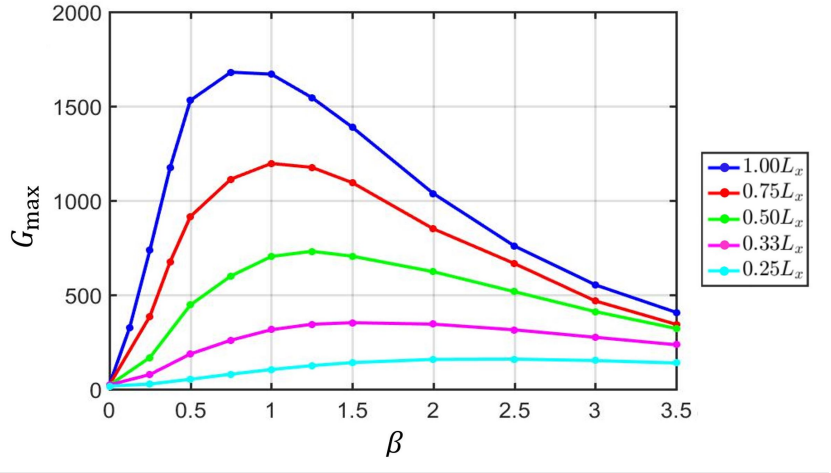

Figure 10: Maximum transient energy growth versus spanwise wavenumber for five different streamwise domain lengths where $L_x = 235\delta_{\text{in}}$.

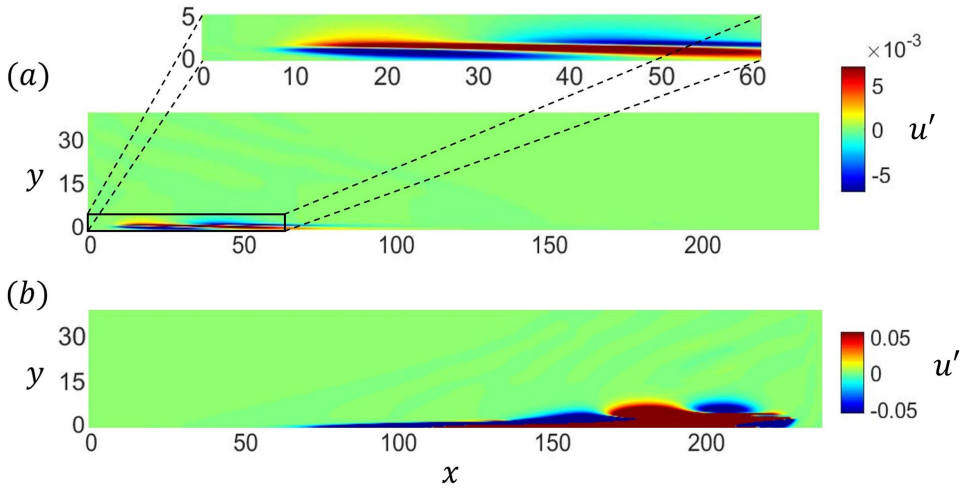

Figure 11: Optimal (a) initial and (b) final states corresponding to Figure 10.

Figure 10 displays the maximum transient energy growth versus spanwise wavenumber for several streamwise domain lengths. These plots were generated by taking the maximum of $G(\beta, t)$ in time t and keeping

only the variation with spanwise wavenumber β. For the range of parameters considered, we know from Figure 10 that a Mach 5.92 spatially developing boundary layer with $Re_{\delta_{in}} = 9660$ can obtain a peak transient growth of 1680 at $t = 175$, $\beta = 0.75$, and $L_x = 235\delta_{\text{in}}$. We show the optimal initial and final states at these conditions in Figure 11. The initial state is comprised of elongated streamwise structures near the left inlet that are tilted against the mean shear of the boundary layer. Notice that these streamwise streaks in Figure 11(a) have a very shallow angle due to the high-speed nature of the flow. These tilted streamwise streaks will start to align themselves with the mean shear as time passes causing substantial growth. This is commonly referred to as the inviscid Orr mechanism.[13] It has been shown before by Butler and Farrell[12] that these types of elongated streamwise structures grow rapidly and robustly. We see by comparing Figure 11(a) to Figure 11(b) that there is significant transient growth. The final state is also comprised of streamwise streaks that extend to the right outlet.

The lift-up effect is the dominant transient growth mechanism for a Mach 2.5 parallel boundary layer with streamwise wavenumber $\alpha = 0$. However, for a Mach 5.92 spatially developing boundary layer, the Orr mechanism and convective instabilities are responsible for the optimal transient response. For higher Mach number flows, it is well-known that 2nd-mode instability becomes more prevalent.[50] Here, 2nd-mode instability refers to a trapped acoustic wave inside the boundary layer. An impulse response could provide more information about what types of convective instabilities are present in this flow.

C. Shock wave/boundary layer interactions

As shown in the previous section, a simple flat plate boundary layer at Mach 5.92 supports significant transient growth. In this section, we consider a SWBLI at precisely the same conditions, to examine its effect on transient growth. As we will show, SWBLI alters the mechanisms responsible for transient growth, and significantly enhances the overall growth that is possible in an otherwise globally stable flow.

We compute a steady two-dimensional base flow of an oblique shock wave/laminar boundary layer interaction at Mach 5.92 with the US3D hypersonic flow solver.[51] The incident oblique shock wave is introduced by modifying the inlet boundary layer profile so that the Rankine-Hugoniot jump conditions are satisfied at the point it enters the domain. We select this point so that the oblique shock impinges upon the wall at a fixed distance of $119\delta^*$ from the leading edge. This ensures that the Reynolds number Re at the impingement point is constant for various shock angles. For this study, we are only interested in an oblique shock angle of $\theta = 13°$. The other boundary conditions are explained in Section IIIB because they are used for the spatially developing boundary layer with no incident oblique shock wave. We also employ the same grid used earlier for the nonparallel boundary layer.

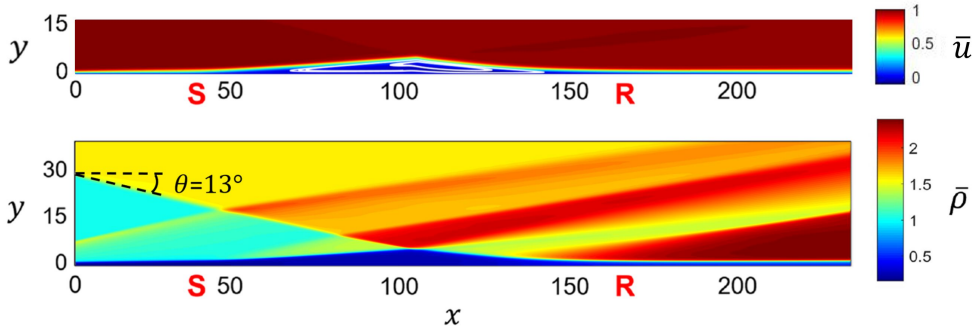

Figure 12: Contour plots of streamwise velocity and density for a Mach 5.92 SWBLI with an incident shock angle of $\theta = 13°$. Here, S and R represent the separation and reattachment points, respectively. The white contours indicate streamlines inside the recirculation bubble.

Figure 12 depicts the SWBLI base flow with color contours of streamwise velocity and density. We nondimensionalize x, y, and z by the displacement thickness δ_{in}. The incident oblique shock wave causes the boundary layer to separate from the wall at $x \approx 50$. Around this location, we observe that a reflected shock wave forms. The separated boundary layer causes a recirculation bubble to develop which has nearly constant density. At the apex of the recirculation bubble, an expansion fan forms and extends up into the freestream. At $x \approx 155$, the flow reattaches to the wall and compression waves coalesce to form a second

reflected shock. Figure 12(b) also shows a bow shock that enters the domain through the left inlet. This bow shock is created by the leading edge of the flat plate and it does not interact with the recirculation bubble.

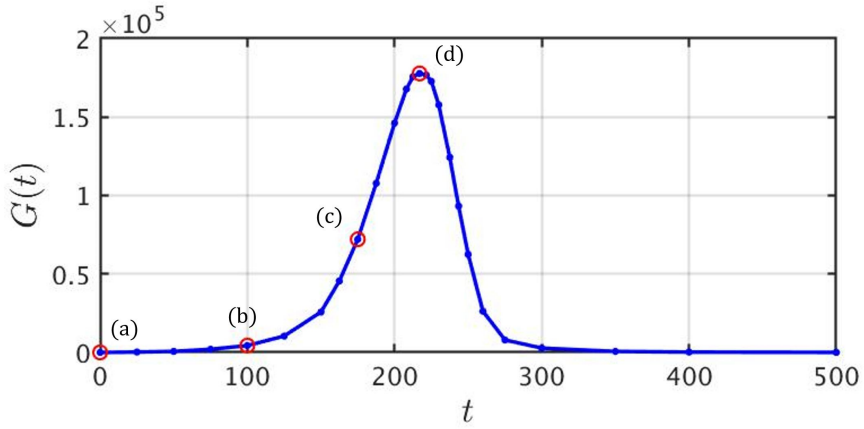

Figure 13: Envelope of the optimal transient energy growth $G(t)$ for a Mach 5.92 SWBLI with incident shock angle $\theta = 13°$ and spanwise wavenumber $\beta = 0.75$.

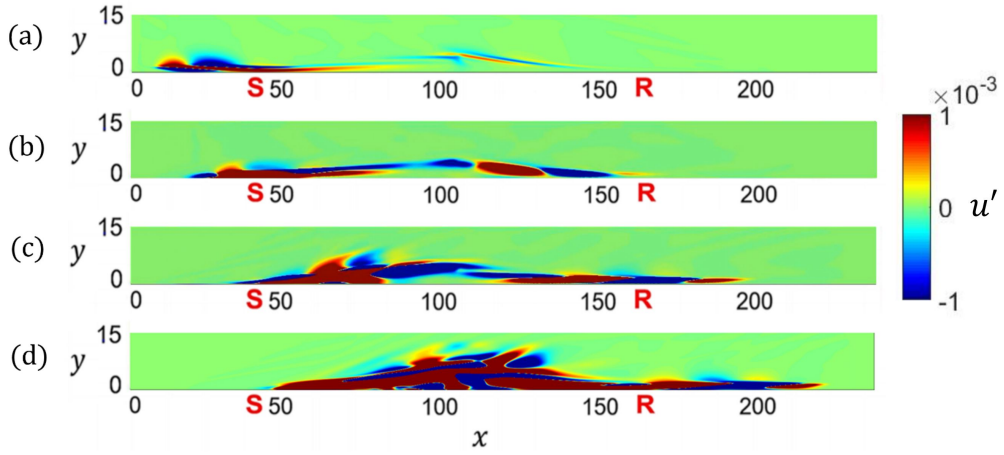

Figure 14: Optimal states corresponding to the labels in Figure 13. The initial state is denoted with (a) and the final state with (d).

Recent work by Dwivedi et al.[27] measured the spatial growth of elongated streamwise streaks after the reattachment point of oblique shock wave/laminar boundary layer interactions using a PSE-based looping approach. Since the parabolized stability equations require a slowly varying base flow,[54] this approach can not be applied within the recirculation bubble. However, the global adjoint looping method described in Section IID requires no such assumption. Therefore, it can be applied to the entire two-dimensional steady base flow in Figure 12. We show the transient growth envelope of this base flow at $\beta = 0.75$ in Figure 13. It is important to note that $\beta = 0.75$ is the nondimensional spanwise wavenumber that corresponds to the optimal transient growth for the spatially developing boundary layer in Figure 8. The maximum value $G(t)$ obtains is 1.78×10^5 at $t = 217$ in Figure 13, which is roughly two orders of magnitude larger than the transient growth seen in Figure 10. After time $t = 217$, the transient growth $G(t)$ decreases to zero because the SWBLI is globally stable at these conditions.[7] The transient growth $G(t)$ is equal to unity when $t = 0$ because of its definition written out in equation (9).

We show the optimal initial and final states of the Mach 5.92 SWBLI with $\theta = 13°$ and $\beta = 0.75$ in Figure 14. There are also two intermediary states plotted, one at $t = 100$ and the other at $t = 175$. We see tilted streamwise streaks near the left inlet in Figure 14(a). These elongated streamwise structures

align themselves with the mean shear in Figure 14(c) causing substantial transient growth. In Figure 14(b), perturbations near the apex of the recirculation bubble start to grow dramatically. These perturbations turn into long streamwise streaks that flow out of the domain in Figures 14(c) and 14(d). Centrifugal instability significantly contributes to the growth of these perturbations.[7] Both the Landahl lift-up effect and the inviscid Orr mechanism could be responsible for the optimal transient response of a SWBLI. Another possible growth mechanism is Kelvin-Helmholtz instability since there is a shear layer that forms once the boundary layer separates. More calculations need to be done in order to determine what growth mechanisms (including convective instabilities) provide a meaningful contribution.

IV. CONCLUSIONS

We applied a nonmodal optimal transient growth analysis to parallel and nonparallel boundary layers. Near the end of our paper, we show some preliminary results from applying this transient growth analysis to oblique shock wave/laminar boundary layer interactions. To compute the optimal transient growth $G(t)$, we employed an adjoint looping approach (see Figure 2) that is described thoroughly in an annual review paper by Schmid.[39] This approach converges quickly (see Appendix) allowing for several runs needed to trace out transient growth envelopes and investigate the impact of different streamwise and spanwise wavenumbers. Convective-type instabilities, the inviscid Orr mechanism,[13] and the Landahl lift-up effect,[17,18] are found to be responsible for large transient growth in high-speed boundary layers.

A verification of our adjoint looping method against a few test cases in Hanifi et al.[19] provided valuable insight. This involved computing transient growth envelopes of parallel boundary layers as well as finding the optimal initial and final states. From Figures 4, 5, and 7, we see that there is good agreement between our nonmodal adjoint looping method and a modal singular value decomposition. We also found that the Landahl lift-up effect[17,18] is the dominant growth mechanism in a parallel boundary layer flow with streamwise wavenumber $\alpha = 0$ agreeing with previous studies.[8,19] Since a modal singular value decomposition about complex boundary layer flows occasionally takes thousands of eigenmodes to converge,[36] the nonmodal adjoint looping approach used in this study provides a nice alternative.

We consider a spatially developing boundary layer in this work as an intermediate step between parallel boundary layer flows and transitional SWBLIs. From Figure 10, the transient growth $G(t)$ increases significantly in a nonparallel boundary layer with longer streamwise domain lengths. This indicates that a Mach 5.92 spatially developing boundary layer with $Re = 9660$ is convectively unstable. Therefore, localized perturbations introduced upstream will grow as they convect downstream without causing the system to become globally (or absolutely) unstable. More specifically, a trapped acoustic wave inside the boundary layer (or 2nd-mode instability) could be responsible for the large transient growth.[50] For a spatially developing boundary layer, the inviscid Orr mechanism[13] also contributes to the optimal transient response. In other words, tilted streamwise streaks near the inflow align themselves with the mean shear of the boundary layer as time passes causing substantial growth.

Finally, we compute the optimal transient growth of a Mach 5.92 oblique shock wave/laminar boundary layer interaction with $Re = 9660$. Another benefit of the global adjoint looping method is that it lets perturbations propagate upstream and downstream, unlike methods based on the parabolized stability equations. This allows us to capture the physics associated with the recirculation bubble and understand how it changes the transient growth. Figure 13 shows that the optimal $G(t)$ is around several orders of magnitude larger than the transient growth in a spatially developing boundary layer. The optimal initial condition could be related to both the inviscid Orr mechanism and the lift-up effect. Figure 14(a) shows that tilted streamwise streaks are present in the upstream boundary layer. Centrifugal instability contributes to the formation of elongated streamwise structures downstream.[7] Since this oblique shock wave/laminar boundary layer interaction has several competing nonmodal transient growth mechanisms, more calculations and analyses need to be performed in the future.

Appendix

Since the adjoint looping approach in Figure 2 only solves for one point on a transient growth curve, it takes several iterations of this approach to trace out a full envelope (see Figures 4 and 5). In order to include variations with respect to the streamwise or spanwise wavenumber (see Figure 9), this adjoint looping approach has to be repeated hundreds of times. We show the convergence history of this iterative

approach for a Mach 5.92 SWBLI with $\theta = 13°$ and $\beta = 0.75$ at $t = 175$. Notice that it takes approximately 5-6 iterations to converge to the optimal initial and final states. This corresponds to a wait time of about 2-3 minutes. The convergence for parallel and nonparallel boundary layers is similar. We know that the convergence depends on the given initial condition. For this study, we use a randomly generated flow field with unit energy norm, but a Gaussian pulse or another type of initial disturbance could take much longer to converge. Further, other optimization techniques (for example, conjugate gradient algorithms) could speed up convergence even more.

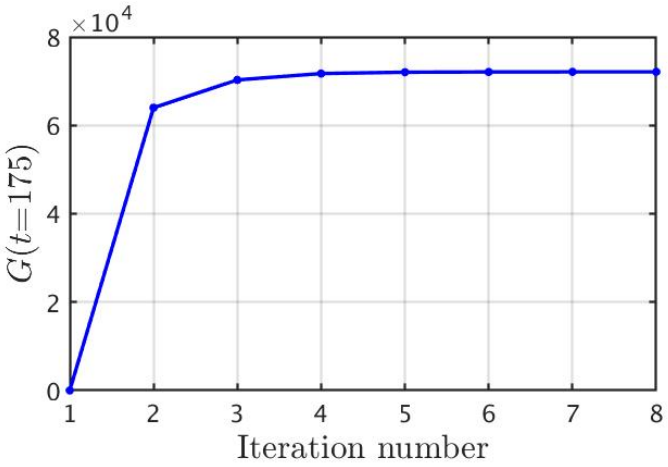

Figure 15: Convergence of the adjoint looping method in Figure 2 for a Mach 5.92 SWBLI with $\theta = 13°$ and $\beta = 0.75$. This corresponds to label (c) in Figure 13.

Acknowledgments

We are very grateful to the Office of Naval Research for their support of this study through grant number N00014-15-1-2522. Thanks to Anubhav Dwivedi at the University of Minnesota for providing the base flows from US3D. Conversations with Pedro Paredes, Meelan Choudhari, and other scientists at the NASA Langley Research Center are also greatly appreciated.

References

[1]Mack, L. M., "Computations of the stability of the laminar compressible boundary layer," *Methods in Computational Physics*, edited by B. Alder, S. Fernback, and M. Rotenberg, Vol. 4, Academic Press, New York, 1965, pp. 247-299.

[2]Mack, L. M., "Boundary layer stability theory," Tech. Rep. JPL-900-277-REV-A; NASA-CR-131501, Jet Propulsion Laboratory, California Institute of Technology, 1969.

[3]Reshotko, E., "Boundary-Layer Stability and Transition," *Annual Review of Fluid Mechanics*, Vol. 8, No. 1, 1976, pp. 311-349.

[4]Theofilis, V., Hein, S., and Dallmann, U., "On the origins of unsteadiness and three-dimensionality in a laminar separation bubble," *Philosophical Transactions of the Royal Society A*, Vol. 358, 2000, pp. 3229-3246.

[5]Robinet, J.-Ch., "Bifurcations in shock-wave/laminar-boundary-layer interaction: global instability approach," *Journal of Fluid Mechanics*, Vol. 579, 2007, pp. 85-112.

[6]Rodriguez, D. and Theofilis, V., "Structural changes of laminar separation bubbles induced by global linear instability," *Journal of Fluid Mechanics*, Vol. 655, 2010, pp. 280-305.

[7]Hildebrand, N., Dwivedi, A., Nichols, J. W., Jovanović, M. R., and Candler, G. V., "Simulation and stability analysis of oblique shock-wave/boundary-layer interactions at Mach 5.92," *Physical Review Fluids*, Vol. 3, No. 1, 2018.

[8]Bitter, N. P. and Shepherd, J. E., "Transient growth in hypersonic boundary layers," AIAA Paper No. 2014-2497, June 2014, pp. 1-18.

[9]Andersson, P., Berggren, M., and Henningson, D. S., "Optimal disturbances and bypass transition in boundary layers," *Physics of Fluids (1994-present)*, Vol. 11, No. 1, 1999, pp. 134-150.

[10]Trefethen, L., Trefethen, A., Reddy, S., and Driscoll, T., "Hydrodynamic Stability Without Eigenvalues," *Science*, Vol. 261, No. 5121, 1993, pp. 578-584.

[11]Hultgren, L. S. and Gustavsson, L. H., "Algebraic growth of disturbances in a laminar boundary layer, *Physics of Fluids (1958-1988)*, Vol. 24, No. 6, 1981, pp. 1000-1004.

[12]Butler, K. M. and Farrell, B. F., "Three-dimensional optimal perturbations in viscous shear flow, *Physics of Fluids A: Fluid Dynamics (1989-1993)*, Vol. 4, No. 8, 1992, pp. 1637-1650.

[13]Orr, W. M. F., "The stability or instability of the steady motions of a perfect liquid and of a viscous liquid. Part I: A perfect liquid. Part II: A viscous liquid., *Proc. R. Irish Acad.*, Vol. 27, 1907, pp. 9-138.

[14]Luchini, P., "Reynolds-number-independent instability of the boundary layer over a flat surface," *Journal of Fluid Mechanics*, Vol. 327, 1996, pp. 101-115.

[15]Luchini, P., "Reynolds-number-independent instability of the boundary layer over a flat surface: optimal perturbations," *Journal of Fluid Mechanics*, Vol. 404, 2000, pp. 289-309.

[16]Tempelmann, D., Hanifi, A., and Henningson, D. S., "Spatial optimal growth in three-dimensional boundary layers," *Journal of Fluid Mechanics*, Vol. 646, 2010, pp. 5-37.

[17]Landhal, M. T., "Dynamics of boundary layer turbulence and the mechanism of drag reduction," *Physics of Fluids (1958-1988)*, Vol. 20, No. 10, 1977, pp. 55-63.

[18]Landhal, M. T., "A note on an algebraic instability of inviscid parallel shear flows,"," *Journal of Fluid Mechanics*, Vol. 98, No. 2, 1980, pp. 243-251.

[19]Hanifi, A., Schmid, P. J., and Henningson, D. S., "Transient growth in compressible boundary layer flow," *Physics of Fluids*, Vol. 8, 1996, pp. 826-837.

[20]Tumin, A. and Reshotko, E., "Spatial theory of optimal disturbances in boundary layers," *Physics of Fluids*, Vol. 13, No. 7, 2001, pp. 2097-2104.

[21]Tumin, A. and Reshotko, E., "Optimal disturbances in compressible boundary layers," *AIAA Journal*, Vol. 41, No. 12 2003, pp. 2357-2363.

[22]Zuccher, S., Tumin, A. and Reshotko, E., "Parabolic approach to optimal perturbation in compressible boundary layers," *Journal of Fluid Mechanics*, Vol. 556, 2006, pp. 189-216.

[23]Tempelmann, D., Hanifi, A., and Henningson, D. S., "Spatial optimal growth in three-dimensional compressible boundary layers," *Journal of Fluid Mechanics*, Vol. 704, 2012, pp. 251-279.

[24]Paredes, P., Choudhari, M. M., Li, F., and Chang, C.-L., "Transient growth analysis of compressible boundary layers with parabolized stability equations," AIAA Paper No. 2016-0051, January 2016, pp. 1-20.

[25]Paredes, P., Choudhari, M. M., Li, F., Jewell, J. S., Kimmel, R. L., Marineau, E. C., and Grossir, G., "Nosetip Bluntness Effects on Transition at Hypersonic Speeds: Experimental and Numerical Analysis Under NATO STO AVT-240," AIAA Paper No. 2018-0057, January 2018, pp. 1-25.

[26]Guiho, F., Alizard, F., and Robinet, J.-Ch., "Instabilities in oblique shock wave/laminar boundary-layer interactions," *Journal of Fluid Mechanics*, Vol. 789, 2016, pp. 1-35.

[27]Dwivedi, A., Nichols, J. W., Candler, G. V., and Jovanović, M. R., "Optimal spatial growth of streaks in oblique shock/boundary layer interaction," AIAA Paper No. 2017-4163, June 2017, pp. 1-13.

[28]Sartor, F., Mettot, C., Bur, R., and Sipp, D., "Unsteadiness in transonic shock-wave/boundary-layer interactions: experimental investigation and global stability analysis," *Journal of Fluid Mechanics*, Vol. 781, 2015, pp. 550-577.

[29]Corbett, P. and Bottaro, A., "Optimal linear growth in swept boundary layers," *Journal of Fluid Mechanics*, Vol. 435, 2001, pp. 1-23.

[30]Shrestha, P., Dwivedi, A., Hildebrand, N., Nichols, J. W., Jovanović, M. R., and Candler, G. V., "Interaction of an oblique shock with a transitional Mach 5.92 boundary layer," AIAA Paper No. 2016-3647, June 2016, pp. 1-14.

[31]Semper, M. T., Pruski, B. J., and Bowersox, R. D. W., "Freestream turbulence measurements in a continuously variable hypersonic wind tunnel," AIAA Paper No. 2012-0732, June 2012, pp. 1-13.

[32]Sesterhenn, J., "Bifurcations in shock-wave/laminar-boundary-layer interaction: global instability approach," *Computers and Fluids*, Vol. 30, No. 1, 2000, pp. 37-67.

[33]Nichols, J. W. and Lele, S. K., "Global modes and transient response of a cold supersonic jet," *Journal of Fluid Mechanics*, Vol. 669, 2011, pp. 225-241.

[34]Malik, M. R., "Numerical methods for hypersonic boundary layer stability," *Journal of Computational Physics*, Vol. 86, No. 2, pp. 376-413.

[35]Schmid, P. J. and Henningson, D. S., *Stability and Transition in Shear Flows*, Springer, New York, 2001.

[36]Akervik, E., Ehrenstein, U., Gallaire, F., and Henningson, D. S., "Global two-dimensional stability measures of the flat plate boundary layer flow," *European Journal of Mechanics*, Vol. 27, No. 5, 2008, pp. 501-513.

[37]Luchini, P. and Bottaro, A., "Adjoint Equations in Stability Analysis," *Annual Review of Fluid Mechanics*, Vol. 46, 2013, pp. 493-517.

[38]Chu, B.-T., "On the energy transfer to small disturbances in fluid flow (Part I)," *Acta Mechanica*, Vol. 1, 1965, pp. 215-234.

[39]Schmid, P. J., "Nonmodal Stability Theory," *Annual Review of Fluid Mechanics*, Vol. 39, 2007, pp. 129-162.

[40]Hill, D., "Adjoint systems and their role in the receptivity problem for boundary layers," *Journal of Fluid Mechanics*, Vol. 292, 1995, pp. 183-204.

[41]Guégan, A., Schmid, P. J., and Huerre, P., "Optimal energy growth and optimal control in swept Hiemenz flow," *Journal of Fluid Mechanics*, Vol. 566, 2006, pp. 11-45.

[42]Pralits, J. O., Airiau, C., Hanifi, A., and Henningson, D. S., "Sensitivity analysis using adjoint parabolized stability equations for compressible flows," *Flow Turbulence and Combustion*, Vol. 65, 2000, pp. 321-346.

[43]Subbareddy, P. K. and Candler, G. V., "A fully discrete, kinetic energy consistent finite-volume scheme for compressible flows," *Journal of Computational Physics*, Vol. 228, No. 5, 2009, pp. 1347-1364.

[44]Ducros, F., Ferrand, V., Nicoud, F., Weber, C., Darracq, D., Gacherieu, C., and Poinsot, T., "Large-eddy simulation of the shock/turbulence interaction," *Journal of Computational Physics*, Vol. 152, No. 2, 1999, pp. 517-549.

[45]Wright, M. J., Candler, G. V., and Prampolini, M., "Data-parallel lower-upper relaxation method for the Navier-Stokes equations," *AIAA Journal*, Vol. 34, No. 7, 1996, pp. 1371-1377.

[46]Wright, M. J., Candler, G. V., and Bose, D., "Data-parallel line relaxation method for the NavierStokes equations," *AIAA Journal*, Vol. 36, No. 9, 1998, pp. 1603-1609.

[47]Nichols, J. W., Lele, S. K., and Moin, P., "Global mode decomposition of supersonic jet noise," Center for Turbulence Research, Annual Research Briefs, Stanford University, 2009, pp. 3-15.

[48]Li, X. S. and Demmel, J. W., "SuperLU_DIST: a scalable distributed memory sparse direct solver for unsymmetric linear systems," *ACM Transactions on Mathematical Software*, Vol. 29, No. 2, 2003, pp. 110-140.

[49]Mani, A., "On the reflectivity of sponge zones in compressible flow simulations," Center for Turbulence Research, Annual Research Briefs, Stanford University, 2010, pp. 117-133.

[50]Bitter, N. P., Ph.D. Thesis, California Institute of Technology, 2015.

[51]Candler, G. V., Subbareddy, P. K., and Nompelis, I., in *CFD Methods for Hypersonic Flows and Aerothermodynamics*, edited by E. Josyula (AIAA, Virginia, 2015), pp. 203-237.

[52]Cossu, C. and Chomaz, J.-M., "Global measures of local convective instabilities," *Physical Review Letters*, Vol. 78, 1997, pp. 4387-4390.

[53]Nichols, J. W. and Lele, S. K., "Non-normal global modes of high-speed jets," *International Journal of Spray and Combustion Dynamics*, Vol. 3, No. 4, 2011, pp. 285-302.

[54]Herbert, T., "Parabolized Stability Equations," *Annual Review of Fluid Mechanics*, Vol. 29, 1997, pp. 245-283.